

RESEARCH

Open Access



Characterization of the symmetrical benzimidazole twin drug TL1228: the role as viral entry inhibitor for fighting COVID-19

Michela Murdocca^{1†}, Osvaldo Andrade Santos-Filho^{2†}, Claudia De Masi¹, Edivaldo dos Santos Rodrigues², Claudia Valeria Campos de Souza², Riccardo De Santis^{3,4}, Donatella Amatore⁴, Andrea Latini¹, Rossella Schipani¹, Lino di Rienzo Businco⁵, Bruno Brandimarte⁶, Giorgia Grilli⁴, Tien L Huang⁷, Annie S Mayence⁷, Florigio Lista⁴, Andrea Duranti⁸, Federica Sangiuolo^{1*}, Jean Jacques Vanden Eynde⁹ and Giuseppe Novelli¹

Abstract

The severe acute respiratory syndrome coronavirus 2 (SARS-CoV-2) is reliably one of the largest pandemics the world has suffered in recent years. In the search for non-biological antivirals, special emphasis was placed on drug repurposing to accelerate the clinical implementation of effective drugs.

The life cycle of the virus has been extensively investigated and many human targets have been identified, such as the molecular chaperone GRP78, representing a host auxiliary factor for SARS-CoV-2 entry. Here we report the inhibitor capacity of TL1228, a small molecule discovered through an *in silico* screening approach, which could interfere with the interaction of SARS-CoV-2 and its target cells, blocking the recognition of the GRP78 cellular receptor by the viral Spike protein. TL1228 showed *in vitro* the ability to reduce significantly both pseudoviral and authentic viral activity even through the reduction of GRP78/ACE2 transcript levels. Importantly, TL1228 acts in modulating expression levels of innate immunity and as inflammation markers.

Keywords SARS-CoV-2, GRP78, 3CLpro, Molecular docking, Molecular dynamics, Benzimidazole drug

[†]Michela Murdocca and Osvaldo Andrade Santos-Filho contributed equally to this work.

[†]Jean Jacques Vanden Eynde and Giuseppe Novelli equally last names contribution.

*Correspondence:

Federica Sangiuolo
sanguuolo@med.uniroma2.it

¹Department of Biomedicine and Prevention, University of Rome Tor Vergata, Rome, Italy

²Center of Health Sciences Laboratory of Molecular Modelling & Computational Structural Biology Cidade Universitária, Federal University of Rio de Janeiro IPPN, Av. Carlos Chagas Filho 373, Bloco H, Rio de Janeiro 21941-599, RJ, Brazil

³Department of Public Health and Infectious Diseases, University of Rome Sapienza, Rome, Italy

⁴Defence Institute for Biomedical Sciences, Rome 00184, Italy

⁵Otorhinolaryngology Department, Institute of Sport Medicine and Science CONI, Rome, Italy

⁶Electronic Measurements Physics Department, Sapienza University, Rome, Italy

⁷Formerly Division of Basic Pharmaceutical Sciences, College of Pharmacy, Xavier University of Louisiana, 1 Drexel Drive, New Orleans, LA 70125, USA

⁸Department of Biomolecular Sciences, University of Urbino Carlo Bo, Urbino 61029, Italy

⁹Formerly Department of Organic Chemistry (FS), University of Mons-UMONS, 1 place du Parc, Mons 7000, Belgium



Background

The COVID-19 global pandemic determined by severe acute respiratory syndrome coronavirus 2 (SARS-CoV-2) has unquestionably raised a major public health emergency all over the world [1]. The SARS-CoV-2 genome is characterized by high genetic variability that allows rapid viral growth due to higher chance of reinfection and a decreased vaccination efficacy [2, 3]. This results in hard viral eradication, changes in virulence and pathogenicity, and cross-species transmissions. Furthermore, multiple SARS-CoV-2 variants have spread globally over the last three years [3, 4]. To date, newly emerging Omicron lineages are emerging very quickly [5, 6]. These factors still make it crucial to study and work towards the prevention of COVID-19 infection [3, 4, 7–9].

There are still many uncertainties about the future of this infection and what to expect in terms of new drugs against COVID-19 [5, 10–13]. The deep understanding of virus propagation is crucial to explain the successive SARS-CoV-2 variants transmission and virus evolution [4, 14], but also to find new targets for developing therapeutic strategy that can also avoid bypassing vaccine protection [15–17].

The process of virus attachment to host cells and its entry has been thoroughly studied, since blocking the infection upstream could prevent the exponential growth phase of the virus. In fact, the molecular mechanism underlying the entry of SARS-CoV-2 into host cells has demonstrated the interaction between the viral protein SARS-CoV-2 Spike protein (SARS-2-S) and its angiotensin-converting enzyme 2 (ACE2) target, followed by virus-cell membrane fusion [18].

However, a productive infection requires other factors, such as the cleavage of S protein, which allows it to bind its target, processed by a cell surface transmembrane protease, that is serine 2 (TMPRSS2), a member of the type II transmembrane serine protease family. In cultured human lung epithelial cells, an increase of TMPRSS2 expression enhances SARS-CoV-2 infection, whereas the inhibition of TMPRSS2 expression or activity blocks the viral entry [19]. It has been demonstrated that TMPRSS2 is crucial for SARS-CoV-2 diffusion and disease development in vivo as its knockout reduced the spreading and the intensity of lung pathology in a mouse model. In view of this, targeting this protease could be an effective strategy against Covid-19 disease [20]. Although the ACE-Spike interaction has been recognized as the primary mechanism for SARS-CoV-2 entry into the host cell, other entry mechanisms have been investigated on the involvement of additional targets existing in the host cell, such as the GRP78, a 78 kilo-Dalton glucose-regulated protein [15]. In fact, GRP78 could promote the virus entrance through the interaction with the binding domain of the RBD receptor expressed by SARS-CoV-2

or could represent an alternative target in promoting infection [21]. Moreover, it is equipped with a putative site of interaction with the receptor binding domain of SARS-CoV-2, increasing the chance of facilitating virus entry or serve as an alternative target [15]. GRP78 is the main HS70 family member, supporting important protein folding functions. It holds a substrate binding domain which results to be critical for the formation of the protein complex with SARS-2-S and ACE2 on the surface and on the perinuclear region typical of the endoplasmic reticulum in VeroE6-ACE2 cells [15]. Interestingly, Carlos and coll. [15] demonstrated that targeting GRP78 with monoclonal antibody reduced both the number of cells expressing cell surface form of ACE2 (csACE2) and the level of csACE2 [15].

After the S protein binding to its receptor, the fusion of the viral envelope with host cell membrane allows the release of the viral genome into the cytoplasm, resulting in its translation into a large polypeptide (PP) chain. This PP chain is auto-proteolytically cleaved by two viral proteases such as papain like proteases (PLpro) and 3-chymotrypsin like protease (3CLpro). Since the function of 3CLpro is crucial for viral replication, inhibiting its activity could be an effective strategy to block virus propagation, becoming an attractive drug target [22, 23].

Upon virus interaction with the host cells, the pattern recognition receptors (PRRs), engage virus and activate the innate immunity [24]. Blocking the virus propagation would avoid the hyperinflammation typical of COVID-19, due to high production of proinflammatory cytokines, such as interferon (IFN), interleukin 6 (IL-6), tumor necrosis factor α (TNF- α) and C-X-C motif chemokine ligand 10 (CXCL10) [24].

Twin drugs are molecules made by linking two pharmacophore groups through covalent bonds. In the case of identical units, the design strategy involves duplication and, as for compounds made with different entities, the aim is to have a drug with better characteristics than those of the initial molecules in relation to pharmacokinetic and pharmacodynamic properties [25, 26].

Diamidines, and more specifically bis-benzamidines, constitute a group of twin drugs exhibiting well-recognized antifungal and antiparasitic properties. Some commercially developed examples include Berenil™ (diminazene), Brolene™ (propamidine), and Pentacarinat™ (pentamidine).

Those drugs are known to achieve their objectives by firmly binding the DNA minor groove of the nucleus or mitochondria of microorganisms. The strongest affinity was observed for AT-Rich sites, creating complexes that inhibit DNA-dependent enzymes. Whereas that mode of action has been widely exploited for decades [27], such diamidines are now considered for their activity on other biomolecular targets such as ion channels, enzymes, and

specific RNA–protein, DNA–protein, and protein–protein interactions [28]. Despite those successes, the high basicity of the amidine groups remains an unavoidable drawback, pointed as responsible for poor oral bioavailability and side effects, among which pancreatic complications, cardiotoxicity, and hypotension.

In previous studies, we reasoned that incorporating the amidine functions into a conjugated cyclic skeleton would emerge as a structural modification improving the bioavailability and deserving attention. For that purpose, we focused our attention on the benzimidazole system and designed a small library of bis-benzimidazoles linked by alkyl dioxo chains [29].

Although benzimidazoles are essentially commercialized for their antimicrobial activities, there are several promising results concerning their efficacy against viruses affecting the respiratory system. Based on the experimental evidence [29–33], we carried out docking simulation on those bis-benzimidazoles as binding agents to a viral protease (3CLpro) and host proteins (GRP78 and TMPRSS 2) and, based on those calculations, it was selected 2'-[4,4'-(2-hydroxypropane-1,3-diyl)-bis-(4-oxyphenylene)-bis-1*H*-benzimidazole-5-carboxylic acid (TL1228), previously reported among the first selective inhibitors of the dihydrofolate reductase (DHFR) type B1 [34], to evaluate its potential efficacy against SARS-CoV-2 infection.

In this study we demonstrated the efficacy of TL1228 in counteracting the infective activity of both pseudotype and authentic SARS-CoV-2.

Methods

Protein structures

The crystallographic structures of SARS-CoV-2 3CLpro, with a resolution of 2.16 Å (PDB ID: 6LU7) [35], and human GRP78, with a resolution of 2.99 Å (PDB ID: 5E84) [36] and human TMPRSS2, with a resolution of 1.95 Å (PDB ID: 7MEQ), were obtained from the Protein Data Bank (PDB; <https://www.rcsb.org/pdb/>) [37].

The protein preparation followed three steps: (1) the removal of non-essential water molecules; (2) the addition of polar hydrogens to the enzyme; (3) the calculation of partial charges using both Kollman and Gasteiger's approaches. [38, 39].

Molecular docking

Molecular docking simulations were performed with the AutoDock Vina 1.1.2 program [40], using a hybrid scoring function which allows to match the empirical and knowledge-based functions. Grid maps representing the binding site were generated with a 1.0 Å spacing resolution. The grid boxes for each protein system were defined as follows: (a) 3CLpro: with the center at $x = -10.460$ Å, $y = 4.104$ Å, and $z = 73.009$ Å, and the box dimensions

were defined as $x = 30$ Å, $y = 40$ Å, and $z = 25$ Å; (b) GRP78: with the center at $x = -0.698$ Å, $y = 34.230$ Å, and $z = -28.666$ Å, and the box dimensions were defined as $x = 32$ Å, $y = 26$ Å, and $z = 30$ Å; and (c) TMPRSS2: with the center at $x = -10.860$ Å, $y = -3.373$ Å, and $z = 18.869$ Å; and the box dimensions were defined as $x = 14$ Å, $y = 16$ Å, and $z = 20$ Å.

Molecular dynamics simulations

Based on the best docking pose for TL1228 into the bind site of each protein, molecular dynamics simulations were done with the CHARMM36 force field [41] implemented in the GROMACS 2018.1 program [42]. CHARMM General Force field (CGenFF) program was applied to conduct the parametrization of TL1228 [43] and a dodecahedral simulation box, including solvent inside (TIP3P water model) was used for running all simulations. Counterions were added to the system, and periodic boundary conditions were applied.

Each complex was submitted to energy minimization using the steepest descent algorithm, involving 50,000 steps and convergence. Subsequently, two 100 ps molecular dynamics simulations were performed, aiming to balance the IDO1-flavonoid complexes. NVT and NPT ensemble were used in the first and in the second simulation respectively, always keeping constant the simulation temperature at 300 K. When performing the NPT ensemble, the pressure was maintained at 1 bar.

Then the determination of free energies of interaction between TL1228 and each protein (production stage) was performed by 200 ns molecular dynamics simulations. The running conditions were the following: ensemble NPT, where temperature was maintained, using the V-rescale implementation of Berendsen's thermostat [44]. A molecular frame was sampled every 10 ps. To keep the pressure constant, the Parrinello-Rahman pressure coupling method was used [45]; for the long-range treatment, the PME method was used [46].

After running the MDS, free energy calculations were performed using the MM-PBSA method [47].

The time range for the analyses was chosen to be regarding thermodynamics equilibrium based on the RMSD analysis. It was also performed a cluster analysis using the gmx-cluster module in GROMACS. GROMOS method described by Daura et al. [48] was chosen for the cluster sampling procedure. Since the method needs a RMSD cutoff values to identify the similarities among the structures, several runs using cutoff values between 0.5 Å and 2.0 Å in intervals 0.1 Å was done. The final cutoff values were chosen as the values where the number of clusters achieved convergence. For 3CLpro, GRP78 and TMPRSS2 the cutoffs selected were, respectively, 1.45, 1.25 and 1.40 Å.

ADMET and drug-likeness evaluation

In silico study of physicochemical descriptors related to absorption, distribution, metabolism, excretion, and toxicity (ADMET): molecular weight, cLogP, cLogS, number of hydrogen bond acceptor (HBA) and donor (HBD) groups, and topological polar surface area (TPSA), as well as drug-likeness calculation was performed by DataWarrior 5.5.0. [49]

Visualization tools and plots

Molecular Visualization Programs BIOVIA Discovery Studio 2021 (BIOVIA, Dassault Systèmes; 21.1.0; Discovery Studio Visualizer; Dassault Systèmes: San Diego, CA, USA, 2021.), UCSF Chimera [50], and AutoDock Tools [51] were used. Grace plotting tool was used for graphical analysis (Grace. Available online: <https://plasma-gate.weizmann.ac.il/Grace/> (accessed on 12 July 2023).

Cells

The African green monkey kidney Vero E6 cell line (kindly gifted by Spallanzani Institute, Rome, Italy) and lung epithelial cell lines Calu-3 (ATCC HTB-55) were cultured in Minimum Essential Medium Eagle (SIGMA-Aldrich, United Kingdom) supplemented with 10% fetal bovine serum (FBS; Gibco, Thermo Fisher Scientific, Waltham, MA, USA), 1% L-Glutamine (PAA, The Cell Culture Company), 1% Penicillin/Streptomycin (PAA, The Cell Culture Company). Molecular Visualization Programs BIOVIA Discovery Studio 2021 (BIOVIA, Dassault).

Synthesis of TL1228

TL1228 was synthesized under microwave irradiation (Initiator Biotage oven) as previously described [28, 33, 52]. Briefly, it was prepared by an *O*-alkylation of the opportune hydroxybenzaldehyde with 1,3-dibromopropan-2-ol to form intermediate bis-aldehydes, followed by the condensation with 3,4-diaminobenzoic acid (Fig. 1).

Cell proliferation assay

In order to perform the cell proliferation assay, the seed density of Vero E6 cells was 20.000 cells/well in triplicate, into 96-well plates and cultured with medium containing TL1228 at three different concentrations (30, 40, 60 μ M), based on data obtained from IC50 determination analysis. For three consecutive days, cells were collected and hemocytometric counting was performed. The counting has been evaluated for each triplicate by two different operators.

MTS assay

The MTS assay was conducted with the same culture conditions described for the cell proliferation assay (2×10^4 cells/well into 96-well plates, in triplicate). The growth medium was added with TL1228 30, 40, 60 μ M for 24 h. Culture medium was replaced every 24 h. Then, for three consecutive days, the viability test was placed using the CellTiter 9 Aqueous One Solution Cell Proliferation Assay kit (CTB169; Promega, Fitchburg, WI, USA) following the manufacturer's manual. Untreated cells were used for values normalization.

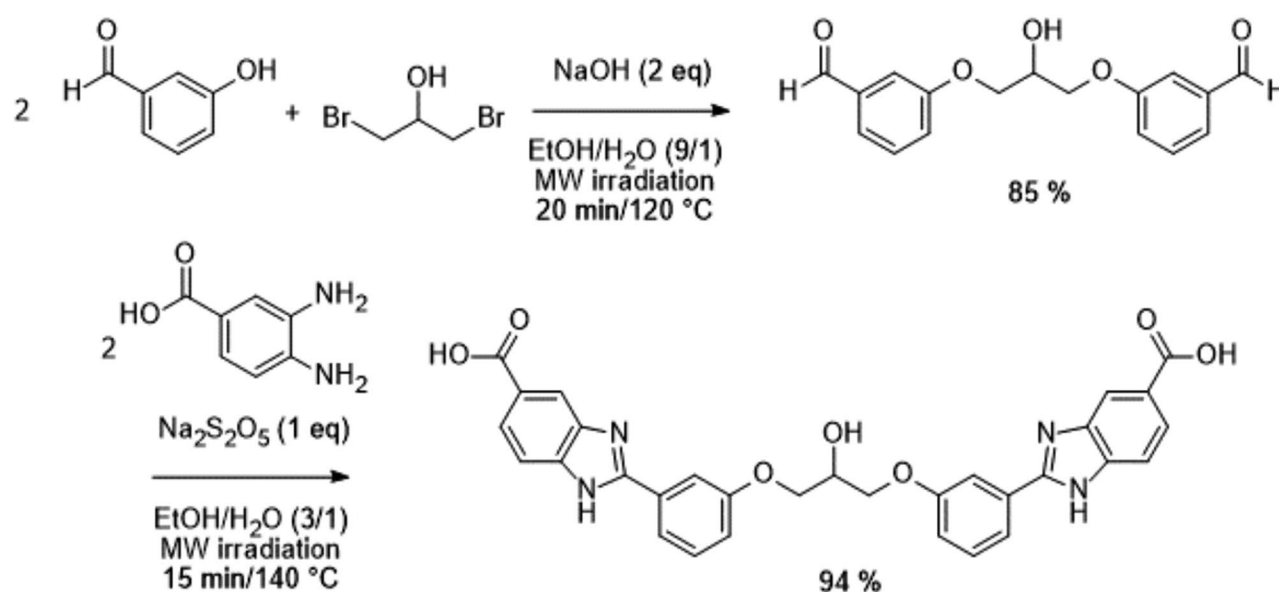


Fig. 1 Synthesis of TL1228. Synthetic procedure to obtain TL1228 under microwave irradiation (Initiator® Biotage oven)

VSV_Pseudo SARS-CoV-2 Omicron BA.4/5, BQ.1.1 and XBB.1.5 strains spike with luciferase reporter

The VSV_Pseudo SARS-CoV-2 S is a construct based on the recombinant vesicular stomatitis virus (Rvsv) engineered to express the Spike protein of SARS-CoV-2 (GenBank: MN908947) with multiple mutations initially identified in the variants of OmicronBA.4/5, BQ.1.1 and XBB.1.5. The pseudovirus infection ability is confined to a single replication viewable by high level luciferase activity.

Determination of TL1228 compound anti VSV_Pseudo SARS-CoV-2 activity

The evaluation of TL1228 anti VSV_Pseudo SARS-CoV-2 activity was assessed employing Vero E6lu-3. The in vitro assays was conducted with the following conditions: 30.000 cells/well in 96-well plates, pre-treated with TL1228 40 μ M for 1 h before the infection. The analysis was conducted using VSV_Pseudo SARS-CoV-2 Omicron BA4/5 (ReVacc Scientific, Cat#P63R98) and BQ1.1 (ReVacc Scientific, Cat# C50J18) in Vero E6 cells and with VSV_Pseudo SARS-CoV-2 Omicron BQ1.1 and XBB.1.5 (ReVacc Scientific, Cat# C50J18;T35V28) in Calu-3. 24 h post-infection, Firefly luciferase activity was assessed using the Promega Luciferase Assay System (E1501) to determine the percentage of infection. Each value was normalized with respect to VSV_Pseudo SARS-CoV-2 alone.

SARS-CoV-2 Virus

SARS-CoV-2 (hCoV-19/Italy/CDG1/2020/EPI_ISL_412,973), isolated from a nasopharyngeal swab by Department of Infectious Diseases, National Institute of Health Rome, and SARS-CoV-2 variant omicron Cerberus (hCoV-19/Italy/LAZ-AMC-07321-DS/2022) isolated from nasopharyngeal swab by Biomedical Institute for Sciences, Rome Italy, were propagated in Vero E6 cells cultured in MEM containing 2% FBS. 72 h after the infection, supernatants containing the released viral particles were collected and centrifuged at 600 g for 5 min. Virus stocks were kept at -80°C until use.

Plaque assay

For the determination of the viral titer, the plaque assay was performed using Vero E6 cells seeded in 12 well-plates at density of 4×10^5 cells/well. After 24 the infection was carried out on the confluent monolayers with SARS-CoV-2. After 1 h at 37°C , the monolayers were washed and the medium was replaced with a mixture of MEM (no glutamine, no phenol-red-GIBCO), 1.5% Tragacanth (SIGMA), NaHCO_3 7% (Gibco), L-glutamine 1X (Gibco), MEM NEAA 1x (Gibco), 0.02 M Hepes (Euroclone), DMSO (Sigma-Aldrich) and 2% FBS (final concentration). 5 days post-infection the plates were washed

with saline solution, stained with 1% crystal violet for 10 min and plaque forming units (PFU) were counted. The plaque reduction ratio was calculated as $(100 - N/N_0 \times 100)$ where N is the PFU count of the treated sample, and N_0 is the PFU count of the control sample.

Antiviral activity

Pre-treatment assay: confluent Vero E6 cell monolayers were treated for 1 h with the compound (TL1228 40 μ M); then the medium was removed, and the infection was performed. 24 h later, the cells monolayer was infected with the collected supernatants for 1 h at 37°C . Then, the inoculum was eliminated, and plaque assay was performed. Untreated-infected cells were used as a positive control of viral infection.

Post-infection treatment assay: Vero E6 cells seeded in a 24-well plate were infected for 1 h at 37°C with SARS-CoV-2 (0.01 m.o.i.); after 1 h incubation, the medium was replaced with fresh medium containing the compound, supplemented with 2% FBS. After 24 h, the supernatants were collected and used to infect cells monolayer for 1 h at 37°C . After the viral adsorption period, the inoculum was removed, and plaque assay was performed. Untreated-infected cells were used as a positive control of viral infection.

Additive treatment assay (Pre+Post): confluent Vero E6 cell monolayers were treated for 1 h with the compound at concentration of 40 μ M; then the medium was removed, and the monolayers were infected for 1 h at 37°C . Then, the inoculum was removed and refreshed with fresh medium containing the compound, supplemented with 2% FBS. After 24 h, the supernatants were collected and used to infect cells monolayer for 1 h at 37°C . After the viral adsorption period, the inoculum was removed, and plaque assay was performed. Untreated-infected cells were used as a positive control of viral infection.

3CL protease activity assay

The activity of 3CL Protease was measured by using the 3CL Protease Assay kit (BPS Bioscience, San Diego, CA, USA). The assay was performed following the manufacturer's instructions.

Gene expression analysis

Total RNAs extraction and the removal of genomic DNA contamination were carried out by Trizol Reagent (Invitrogen Life Technologies Corporation, Carlsbad, CA, US) following manufacturer's instructions and performing the treatment with DNase I-RNase-free (Ambion, Life Technologies Corporation, Foster City, CA, USA). One μ g of RNA was reverse transcribed with the High-Capacity cDNA Archive kit (Life Technologies Corporation, Foster City, CA, USA) and used in RT-qPCR. mRNAs were

measured by SYBR Green (Life Technologies Corporation, Foster City, CA, USA). *GAPDH* was used as reference gene. Primer sequences will be given upon request. The $2^{-\Delta\text{Ct}}$ and comparative $\Delta\Delta\text{Ct}$ methods were used to quantify relative gene expression levels.

Vaporization of TL1228 compound

TL1228 compound 200 μM and 600 μM was vaporized for 10 min over the wells where 1.2×10^5 cells/well had been previously seeded. The medical device used for the micronebulization of the compound was designed by Bruno Brandimarte and built by Ginevri (Rome, Italy; <https://www.ginevri.com>) and DAV Electronics (Twickenham, UK; <https://davelectronics.com>). It has been granted an international patent (#11910772).

After the vaporization, cells were incubated for 1 h at 37 °C and 5% CO_2 and successively infected with a VSV_Pseudovirus carrying the SARS-CoV-2 S protein variant (Omicron XBB.1.5). The efficiency of virus entry was quantified by performing a luciferase assay. Each value was normalized relative to VSV_Pseudo SARS alone (100%).

The in vitro utilization of the device was adapted according to what has been described by Brandimarte et al. [53]. The concentration of the compound TL1228 was increased to 200 μM and 600 μM compared to the one previously used (40 μM) in line with the evidence that aerosolization of compounds, reducing them to smaller particles, is designed to conduct therapeutic agents directly to the alveoli, but in low concentration [53].

Quantification and statistical analysis

All the experiments were performed in technical duplicates, and data were analyzed using GraphPad Prism 8 and the SPSS program, version 25 (IBM Corp, Armonk, NY, USA).

Results

In order to deeply investigate the intermolecular interactions between TL1228 and all three molecular targets (3CLpro, GRP78, and TMPRSS2), as well as to predict the corresponding binding free energies, molecular dynamics simulations (MDS) were carried out for each protein-ligand complex. The root means square deviation (RMSD), radius of gyration (Rg) and root mean square fluctuation (RMSF) analyses are shown in Fig. 2.

Figure 2a and b represent, respectively, the RMSD of the proteins carbons α ($\text{C}\alpha$) and of the TL1228 heavy atoms docked into the proteins binding site. These results show that only TL1228-GRP78 complex presents some considerable instability during the simulation, i.e., the RMSD values range is about 1.5–9.5 Å along the MDS trajectory, while the other protein complexes reach the thermodynamic equilibrium from 50 ns. On the other

hand, as expected, due to its flexible molecular structure, TL1228 shows high RMSD fluctuation during the MDS (Fig. 2b). It is worth of note that TL1228 shows no significative RMSD fluctuation when docked to 3CLpro from ~65 ns (Fig. 2b).

Figure 2c shows the gyration plot for all ligand-protein complexes, and as can be seen, all systems are well structurally packed (folded). The RMSF plots (Fig. 2d) shows that TL1228-GRP78 complex presents more residues fluctuations and TL1228-TMPRSS2 complex presents the smaller residues fluctuation, consistently with a very stable conformation. Regarding the TL1228-3CLpro complex, only the residues 190–194 and the C-terminal of 3CLpro protein, which belongs to loops region, had significative RMSF values (>2.5 Å).

To investigate the interactions made between TL1228 and the proteins, a cluster analysis of the MDS trajectories was performed using the gmx-cluster module of the GROMACS software. The GROMOS method used, described by Dahara and co-workers [47], allows the partitioning of the MDS trajectory structures into clusters based on a root mean square deviation cutoff. The distribution of structures over the RMSD values are shown in Fig. 3a. The TL1228-3CLpro and TL1228-GRP78 complexes have two major clusters, while the TL1228-TMPRSS2 presents only one cluster. For the subsequent ligand-protein interaction analysis, it was considered the most populated cluster for both TL1228-3CLpro and TL1228-GRP78 complexes, and the single cluster for the TL1228-TMPRSS2 complex (Fig. 3b and c, and 3d, respectively). As shown, interactions are responsible for anchoring the compound TL1228 to the binding site of those proteins. Moreover, MM-PBSA approach was used to calculate free energy of binding of TL1228 and each protein. The corresponding results are: 3CLpro (-19.89 kcal/mol); GRP78 (-18.38 kcal/mol); and TMPRSS2 (-21.23 kcal/mol).

In silico ADMET modelling was also carried out, so that some pharmacokinetics, as well as toxicity of compound TL1228, were estimated. The following results were obtained: (a) molecular weight: 564.55; (b) cLogP: 3.56; (c) cLogS: -7.49; (d) polar surface area (PSA): 170.65; (e) mutagenic effect: not detected; (f) tumorigenic effect: not detected; (g) reproductive effect: detected; (h) irritant: not detected; (i) Lipinski rule of five violation (2): molecular weight >500 ; number of N or O: 11 (>10); (h) drug-likeness: 0.36. Based on those values, compound TL1228 has potential to be considered as a lead compound.

Evaluation of TL1228 cytotoxicity in Vero E6 cells

To assess the impact of TL1228 compound on the viability of VERO E6 cells, MTS assay was carried out, following the protocol described in methods. The viability of

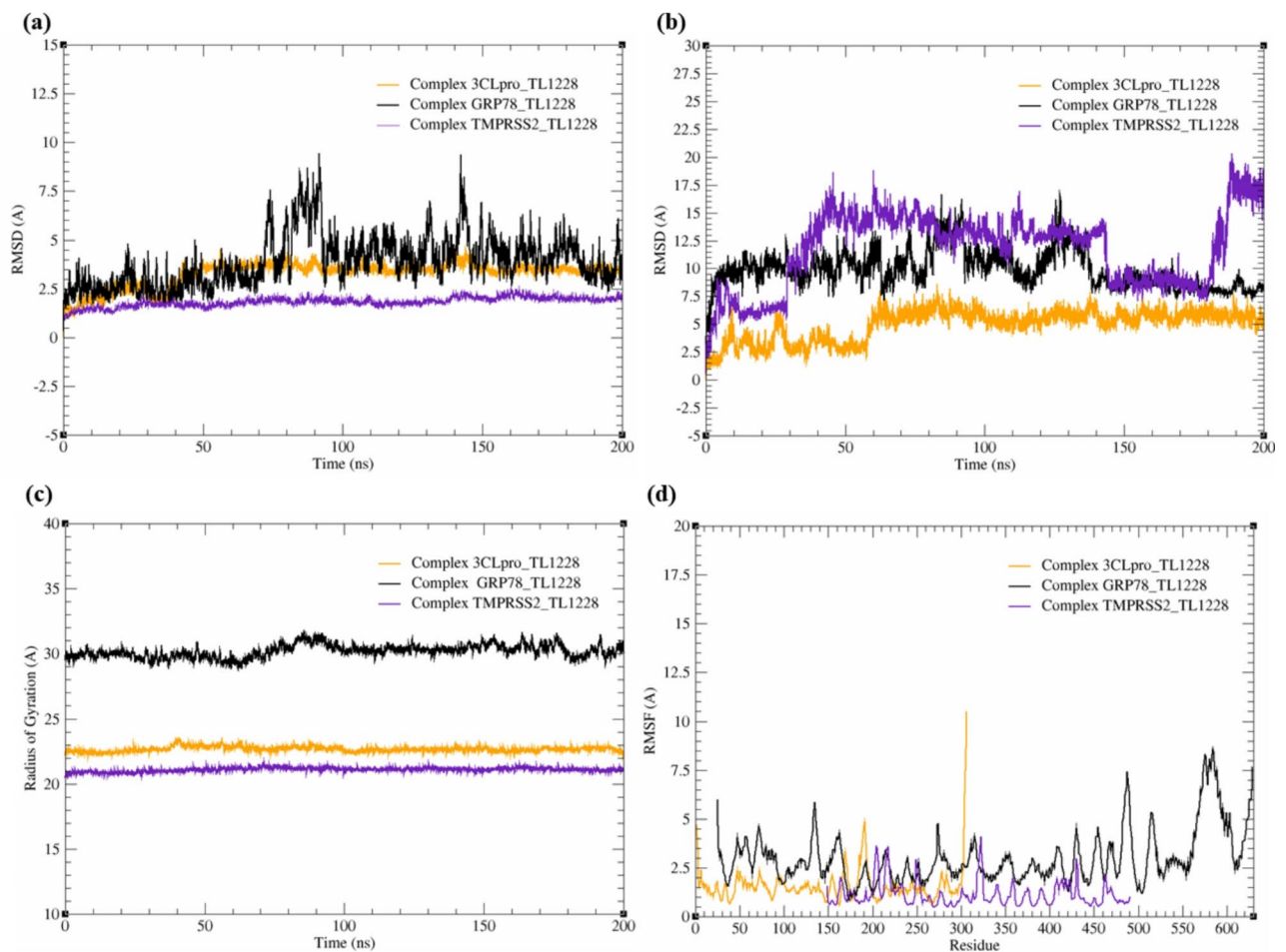


Fig. 2 200 ns MD trajectory analyses. **A** RMSD of the protein carbon α (Ca). **B** RMSD of the TL1228 ligand heavy atoms. **C** Rg of the enzymes Ca. **D** RMSF of the proteins Ca. All simulations were performed in the presence of water molecules, and the used PDB codes for SARS-CoV-2 3CLpro, human GRP78, and human TMRSS2 proteins were, respectively, 6LU7, 5E84, and 7MEQ

cells treated with TL1228 did not show variation among the three different concentrations during the first two days of treatment. However, at day 3 cells treated with the highest concentration (60 μM) of the compound exhibited a statistically significant decrease of viability ($p < 0.05$) compared to untreated once (Fig. 4a). Moreover, VERO-E6 cells were seeded in replicates and counted daily to conduct a time-course analyses of cell proliferation. Figure 4b reports the growth curve of VERO E6 cells treated with 60, 40, 30 μM compared to untreated cells (Ctrl). As shown, 60 μM resulted in cell proliferation slowdown statistically, suggesting that TL1228 at lower concentrations (30 and 40 μM) does not exhibit cytotoxicity.

TL1228 compound hampers the VSV_Pseudo SARS-CoV-2 S Omicron BA.4/5 and BQ1.1 variants in Vero E6 cells

Vero E6 cells were pre-treated with TL1228 (30 and 40 μM) for 1 h to enable the compound acting at once and then infected for 24 h with VSV-Pseudo SARS-CoV-2 S

Omicron BA4/5 and BQ1.1. Analyses were performed after further 24 h from Pseudovirus removal.

The percentage of infection was calculated using the Luciferase assay. The addition of TL1228 compound 30 μM and 40 μM to Omicron BA.4/5 infected cells results in a statistically significant infection reduction to 19.3% and 3.2% respectively (Fig. 5a). The same trend is reproduced also using Omicron BQ1.1 variant, with a percentage of cell infection equal to 20% (TL1228 30 μM) and 3.2% (TL1228 40 μM) (Fig. 5b). Specifically, TL1228 compound 40 μM proves to be more efficient in preventing the ability of both involved variants to trigger the infection (97% of inhibition) than TL1228 30 μM (81% of inhibition). Each value was normalized with respect to VSV_Pseudo SARS-CoV-2 S alone.

TL1228 compound hinder the infection by VSV_Pseudo SARS-CoV-2 S Omicron BQ1.1 and XBB.1.5 in Calu-3 cells

To explore the efficacy of TL1228 compound on human lung epithelial cell lines that can support the propagation

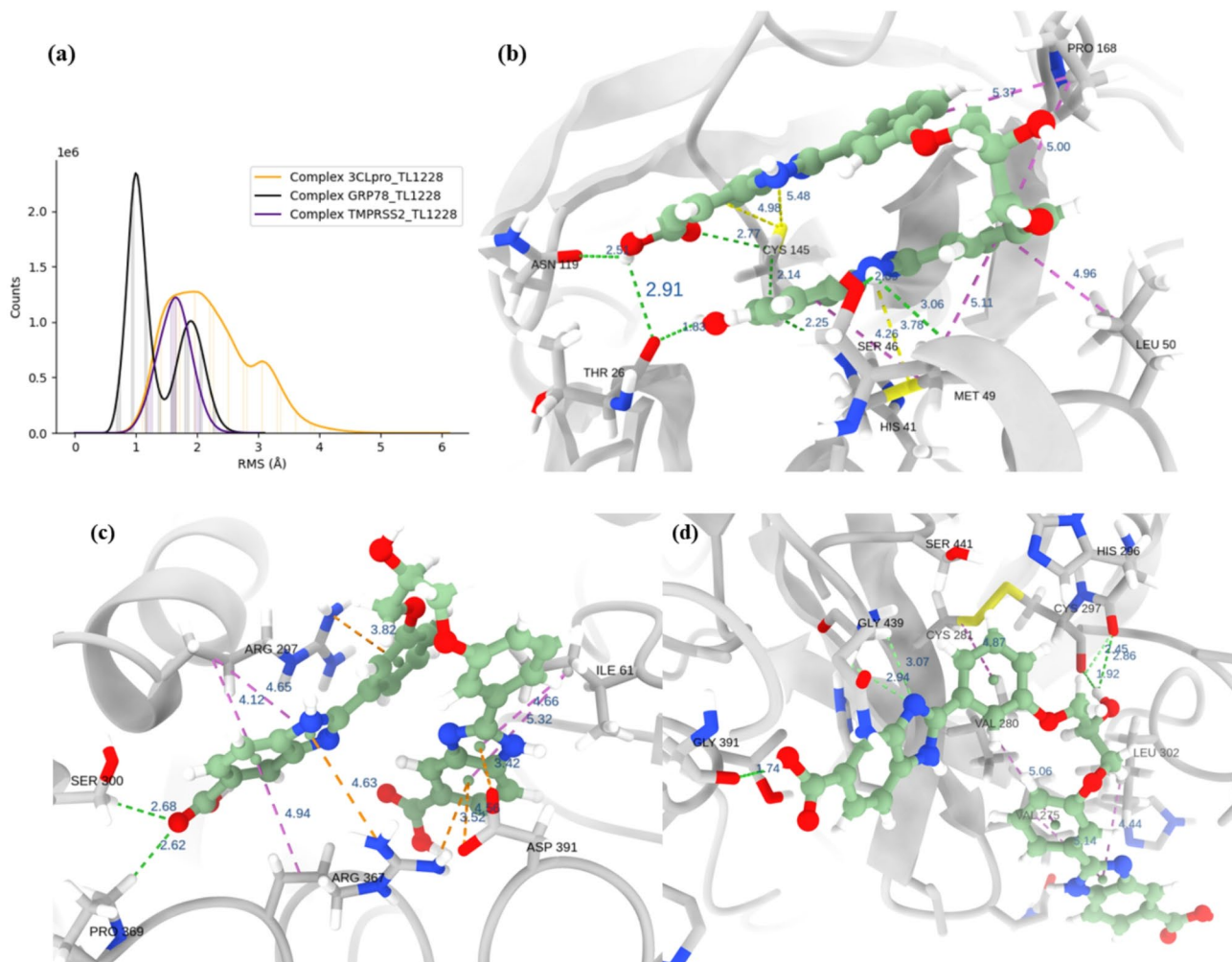


Fig. 3 **A** Cluster distribution for TL1228-protein complexes over RMS values. **B, C, D** key intermolecular interactions (3D representation) between TL1228 and 3CLpro, GRP78, and TMPRSS2, respectively. Colored dashed lines: green: hydrogen bonds; yellow: π -sulfur; orchid: π -alkyl; dark orange: π -anion or π -cation. Protein residues forming just van der Waals interactions with TL1228 show no dashed lines linking to its, but they are labeled in the Figure. The numerical distances (blue) are in angstrom (\AA)

of SARS-CoV-2, Calu-3 cells were infected with VSV_Pseudo SARS-CoV-2 S Omicron BQ1.1 following the same protocol adopted above.

Results confirmed the efficacy of the compound (40 μM) to limit the infection at 20% (Fig. 5c).

Since at the time of the study procedures, the variant VSV_Pseudo SARS-CoV-2 S Omicron XBB.1.5 was spreading, the same experiments were replicated on Calu-3 with this new strain. As shown in the Fig. 5d, the luminescence quantification indicates that the compound has a substantial effect on blocking viral entry, reducing the percentage of infection (13,4%) in a statistically significant manner.

Nebulized TL1228 compound affects VSV_Pseudo SARS-CoV-2 S Omicron XBB.1.5 infection

Since the aerosolized drugs are an important approach to treat pathologic conditions affecting the lungs, TL1228

compound was aerosolized on Calu-3 cells at two different concentrations (200 μM and 600 μM) (Fig. 5e). The compound was pre-vaporized, as describes in methods, over the cell wells before the infection with both VSV_Pseudo SARS-CoV-2 S Omicron BQ1.1 and XBB.1.5. The lower concentration (200 μM) halves the percentage of VSV_Pseudo SARS-CoV-2 S Omicron XBB.1.5 infection, while the highest one (600 μM) decreases this percentage even more, reducing the value to 37% (Fig. 5f). Thus, the nebulization of TL1228 compound is proven to be innovative and particularly effective, as demonstrated in our preliminary results, and it could be useful in improving the therapeutic success of inhalation therapy for COVID-19.

TL1228 impairs SARS-CoV-2 attach and replication

The results obtained prompted us to investigate the antiviral activity of compound TL1228 on SARS-CoV-2

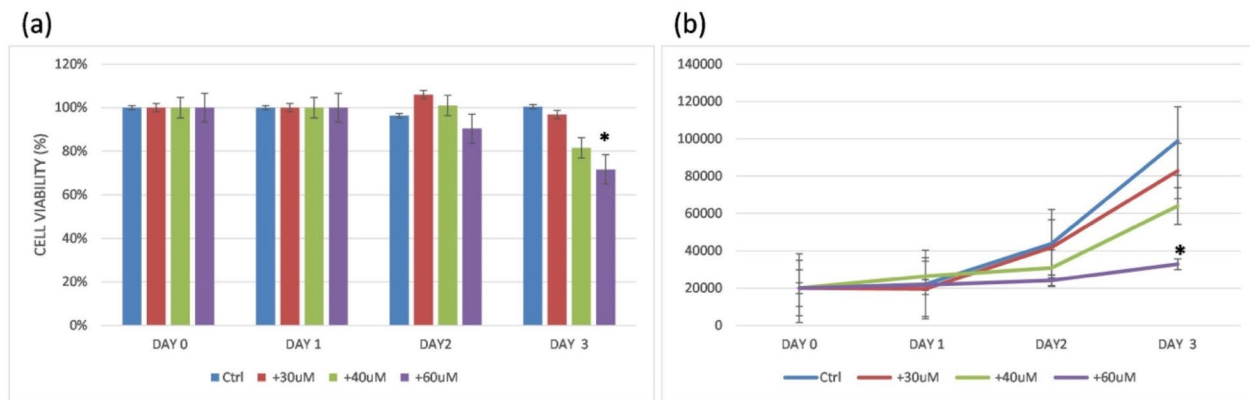


Fig. 4 A Effect of TL1228 compound on the viability of VERO E6 cells for three days. MTS assay was carried out to evaluate cell viability after TL1228 administration at a concentration of 60, 40, 30 μM for 72 h compared to untreated cells. At day 3 the treatment with TL1228 60 μM determined a statistically significant decrease in cell viability ($p < 0.005$). **B** Time course analyses of VERO E6 cell proliferation treated with 60, 40, 30 μM of TL1228 compound. Cells were seeded in replicates and counted daily. Growth curve of cells was elaborated. The data represent the average \pm S.D. of three separate experiments ($*p < 0.05$)

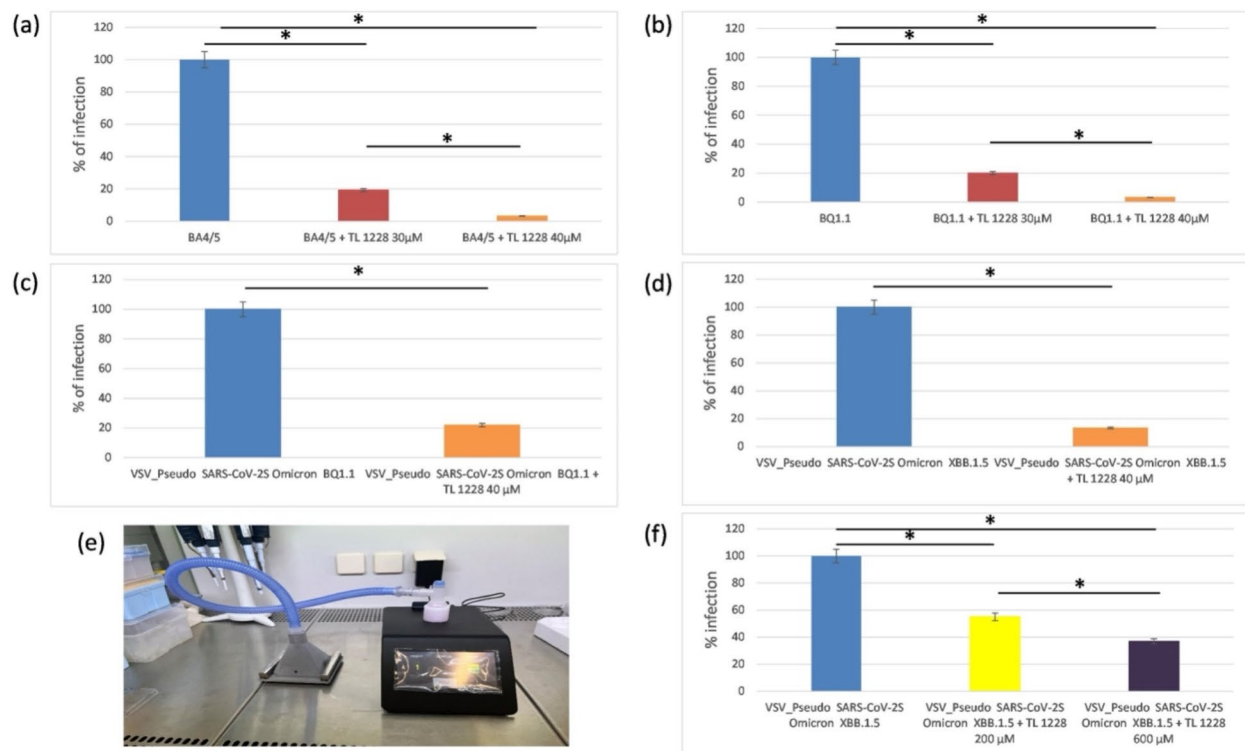


Fig. 5 VeroE6 cells were pre-treated with TL1228 compound (30 and 40 μM) for 1 h and inoculated with pseudotypes particles bearing the S proteins of the indicated variants **A** (Omicron BA.4/5) and **B** (Omicron BQ1.1) for 24 h and then analyzed. Infection efficiency was quantified by measuring virus-encoded luciferase activity in cell lysates after 24 h from Pseudovirus removal and expressed as percentage. Data presented are the average from three biological replicates. Error bars indicate the standard deviation \pm SD. $*p < 0.05$, $**p < 0.01$. Each value was normalized with respect to VSV_Pseudo SARS-CoV-2 S alone. Calu-3 cells were treated previously with TL1228 compound (40 μM) for 1 h and inoculated with pseudotypes particles bearing the S proteins of the indicated variants **C** (Omicron BQ1.1) and **D** (Omicron XBB.1.5) for 24 h and then analyzed. Infection efficiency was quantified by measuring virus encoded luciferase activity in cell lysates after 24 h from Pseudovirus removal and expressed as percentage. Data presented are the average from three biological replicates. Error bars indicate the standard deviation \pm SD. $*p < 0.05$, $**p < 0.01$. Each value was normalized with respect to VSV_Pseudo SARS-CoV-2 S alone. **E** The instrument used for vaporization of TL1228 compound 200 μM and 600 μM . **F** Calu-3 cells infection with VSV-Pseudo-SARS-CoV-2 S Omicron XBB.1.5 and treatment with vaporization of TL1228 compound 200 μM and 600 μM

(hCoV-19/Italy/CDG1/2020/EPI_ISL_412,973). First, it was assessed the effect of compound on cell receptors useful to the virus for entering the cells. To this scope, Vero E6 cells were treated with the TL1228 40 μ M for 1 h at 37 °C. Then, the medium was removed, and a suspension of SARS-CoV-2 was used to infect cell monolayer (see materials and methods). The results demonstrated that cells pre-incubation treatment was able to impair virus entry into host cells. The number of PFU registered in treated-infected cells turned out to be the half respect to that assessed in untreated-infected cells, confirming the data obtained with VSV_Pseudo SARS-CoV-2 S. These findings suggest that the TL1228 compound exerts some activity on the host cell surface and consequently, reduces the ability of the virus to bind the receptor of the host cells (Fig. 6a and b).

In order to verify the effect of the compound on SARS-CoV-2 life cycle, confluent Vero E6 cells were infected with SARS-CoV-2 and, after 1 h incubation, the inoculum was removed and fresh medium containing the compound was added for 24 h. Plaque assay showed that the drug strongly inhibits viral replication by about 90% for both SARS-CoV-2 and BQ.1.1 variant. To evaluate any

possible additive effect of the two treatments, the experiment was performed by pre-incubating the cells with the substance and adding the one after the infection for 24 h. The results demonstrated only a little additive effect with a percentage of inhibition of 94%.

Gene expression Analyses of innate immunity and Inflammation markers in CALU-3 cells

To explore the effect of TL1228 compound on innate immune response and support its efficacy against SARS-CoV-2, we evaluated the immunity-related genes expression in infected Calu-3 cells after TL1228 compound treatment, reporting a significant decrease of type I and III IFNs transcripts, compared to infected cells. TL1228 seems to induce a 6-fold and 2-fold decrease in IFN β and IFN λ 1 expression, respectively reporting values to baseline.

As expected, TL1228 treated Calu-3 cells also showed a downregulation of proinflammatory chemokines and cytokines (CXCL10, IL-6 and TNF- α) (Fig. 6c). Moreover, we also evaluated the potential effect exerted by TL1228 treatment on SARS-Cov2 host receptors mRNA levels, such as ACE2, whose transcript resulted to be

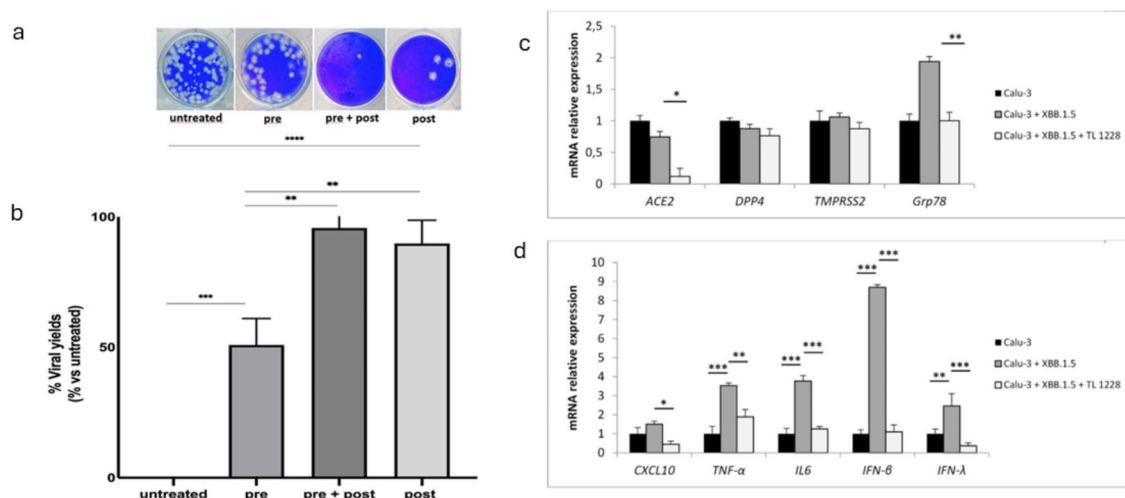


Fig. 6 Inhibition of SARS-CoV-2 (hCoV-19/Italy/CDG1/2020/EPI_ISL_412,973) with the three different treatment assays. Untreated: positive control. Pre: evaluation of inhibition of SARS-CoV-2 entry. Vero E6 were treated with drug at concentration of 40 μ M for 1 h at 37 °C. Post: evaluation of the effect of the compound on SARS-CoV-2 life cycle. Cells were infected for 1 h at 37 °C with SARS-CoV-2 (0.01 m.o.i.) and then treated with the compound for 24 h. Pre + post: evaluation of the two treatments. **A** Plaque assay is performed in the cells infected with the supernatants derived from the cells previously treated. **B** The graph represents the percentage (%) of viral yields vs. untreated virus after the treatments. Data are obtained from at least 3 independent experiments, each performed in triplicate ($n=9$), and are shown as mean \pm SD of the percentage of virus yields vs. untreated (**** $p < 0.0001$; *** $p < 0.001$; ** $p < 0.01$). **C** Targets and **D** immunity-related genes RT-qPCR analyses in Calu-3 cells after XBB.1.5 Pseudovirus infection and following treatment with TL1228 compound. The unit was referred to Calu-3 cells. Data are from three independent experiments and represented as mean \pm SD. * $p < 0.05$, ** $p < 0.01$, and *** $p < 0.001$ by one-way ANOVA test

significantly reduced when compared both to infected and untreated cells (Fig. 6d). Interestingly GRP78 a stress-inducible chaperone, resulted to be upregulated after virus infection as expected, but its expression levels also decreased to basal level after TL1228 treatment (Fig. 6d).

Discussion

A few months after the end of the pandemic, the scientific community was still learning about COVID-19 infection. However, efforts are currently underway to identify new therapeutic targets and the research for molecules that can be effective against COVID-19 infection is very active today [7].

Since the beginning of the pandemic, the urgent need for therapy made the drug repurposing one of the main approaches used to fight the infection [30, 31]. Li and coll. summarized the advancement obtained with COVID-19 drug discovery, based on preclinical and/or clinical studies conducted since the pandemic began, demonstrating that many agents ($n=712$) have an anti-SARS-CoV-2 activity [32]. Most of these compounds are small molecules (53%), followed by antibodies (33%), peptide inhibitors (4%), and others (such as macromolecular inhibitors, RNA-based therapies, and cell-based therapies) [33]. Most agents (>90%) have not progressed towards clinical trials, and lead optimization is still required in most cases [54]. Recently, the outcomes of a phase 2–3, double-blind, randomized, placebo-controlled trial involving Simnotrelvir, an oral 3CLpro inhibitor, have been published [55]. The researchers demonstrated that its early administration shortened the time to the resolution of symptoms among adult patients with COVID-19, without evident safety concerns [55].

SARS-CoV-2, as other RNA viruses, is continually adapting through casual variants [5] leading to important changes in the infectiousness and virulence, and above all, enhancing virus' capacity to evade adaptive immune responses from previous infection or vaccination. There is evidence that some SARS-CoV-2 variants have reduced susceptibility to plasma from people who were previously infected or immunized, as well as to certain anti-SARS-CoV-2 mAbs [56–60].

The early stages of viral infection represent an attractive target for antiviral therapy, as their inhibition can block infection prior to the exponential growth phase of the virus SARS-CoV-2 [57].

In the case of coronaviruses, the Spike protein, plays a crucial role in mediating viral entry and represents a key target for recognition by the host immune system. Moreover, Spike employs ACE2 as a receptor for viral entry, depending on TMPRSS2 protease activity. However, GRP78 is a key ER stress marker crucial for both the entrance and the infectivity of many viruses,

including SARS-CoV-2, thus offering new avenues for antiviral treatments. Carlos and coll. [15] demonstrated that GRP78 is able to form a complex with SARS-CoV-2 Spike protein (S) and ACE2 on both the surface and the perinuclear region typical of the endoplasmic reticulum in VeroE6-ACE2 cells. The substrate binding domain of GRP78 plays a crucial role in this interaction [58]. Notably, GRP78 has been implicated in the entry and replication of various viruses, including Ebola. Therefore, targeting essential auxiliary host chaperones like GRP78, rather than focusing solely on individual viruses susceptible to mutations, could provide a wide variety of antiviral strategies with significant clinical implications beyond SARS-CoV-2. When ER stress occurs in viral infections, GRP78 is overexpressed, it localizes on the surface of cells moving from ER to cell surface, and functions as a virus receptor [21, 59, 60]. A recent molecular docking study has revealed that the spike protein of the SARS-CoV-2 virus has a tight binding affinity with the GRP78 protein, suggesting that this association could be a potential therapeutic strategy for COVID-19.

Based on molecular docking and molecular dynamics simulations, we were able to identify TL1228 as a promising molecular hit among several benzimidazoles previously synthesized by our group. In this context, the docking simulations worked as a tool for virtual screening, and molecular dynamics worked as the tool for investigating the conformational profile, as well as the ligand-proteins binding thermodynamics (free energy calculations). As described in the results above (Figs. 2 and 3), all ligand-protein complexes were kept structurally stable during the time simulations. Moreover, interactions between TL1228 and key protein residues were observed, such 3CLpro catalytic dyad (His41, Cys145), TMPRSS2 triad (His296, Asp345, Ser441), among others.

Regarding the biological assays, the first approach was the evaluation of TL1228 cytotoxicity. The results were in line with the above IC50 determination analysis and allowed us to establish the cut-off concentration to use for the investigation of its potential antiviral activity. The initial hypothesis about the molecular strategy of this promising compound in the execution of its function lies in the good binding affinity to the host proteins GRP78 and TMPRSS2, but also to the viral protease 3CLpro. Starting from this assumption, we decided to pretreat the cells with the compound before the infection, trying to block the receptors able to promote the binding of the S protein to the host cell. The experiments carried out with TL1228 showed an interesting and statistically significant decrease both in Vero E6 and Calu-3 cells infected with three different Pseudovirus strains (BA4/5, BQ.1.1 and XBB.1.1). Successively, these data were also validated in Vero E6 cells infected with live SARS-CoV-2 and variant omicron Cerberus. In fact, the obtained results

demonstrated a viral reduction of about 51% in TL1228 treated infected cells, thus confirming a possible effect of the drug on cell receptors. As the compound had a good affinity for viral protease 3CL-pro, it was investigated the impact of the drug on viral life cycle. Interestingly, post-infection treatment of infected cells caused a significant decrease (90%) of viral titer with respect to that obtained in untreated infected cells, let us to hypothesize that the TL1228 compound can influence the activity of 3CL pro and/or other steps of virus replication cycle. 3CLpro has been implicated in cleaving human immune signaling proteins, indicating its potential to modulate host immune responses [61].

Interestingly, we detected a significant reduction in mRNA levels of IFN β and IFN λ 1 as well as of proinflammatory chemokines and cytokines was observed compared to infected untreated cells.

Furthermore, since GRP78 simplifies the virus entry through ACE2 [15], we investigated if the treatment with TL1228 influences the expression levels of host receptors after infection, but also on inflammatory mediators. Interestingly, a significant reduction of ACE2 transcript levels emerged, probably related to the interaction of TL1228 with GRP78, which in turn returns to baseline levels after treatment.

There is an essential need for a therapeutically effectiveness of easily delivering drugs into the airways. Aerosolized delivery of compounds is an important approach to treat pathologic conditions that primarily affect the lungs. The possibility to administer small molecules that inhibit virus entry opens new possibilities for the prevention and treatment of infectious agents such as SARS-CoV-2.

Thinking about the transposition of TL1228 treatment to in vivo daily life, we performed the experiments with a device able to permit the nebulization of the compound. TL1228 turned out to be effective after vaporization in a significant way, reducing the percentage of infected cells as demonstrated with the Luciferase assay. This could be a great chance to bring, among the anti-Covid therapies, a non-invasive treatment able to reach the respiratory tract and easy to use also in pediatric patients, as preventive measure against the COVID-19 disease manifestation.

TL1228 paves the way for potential prophylactic approaches (e.g., nasal spray) or combinatorial treatments for SARS-CoV-2 infection, though further research is needed. It has demonstrated some antiviral effectiveness against Omicron variants, indicating that future development of more potent compounds in this class could benefit from the multivalent properties, potentially improving resistance to viral escape.

Conclusions

In conclusion, we identified and characterized the antiviral activity and mechanism of action of TL1228 in the inhibition of viral entry, as suggested by molecular docking simulations analyses.

Collectively, even though additional research is mandatory to better understand the compound's mechanism of action, our results highlight that targeting host auxiliary chaperones, such as GRP78 -crucial for viral entry and replication- could offer novel strategies for combating SARS-CoV-2 and potentially other future Coronavirus strains.

Acknowledgements

EdSR thanks the PhD scholarship by Coordenação de Aperfeiçoamento de Pessoal de Nível Superior – Brasil (CAPES), grant number 001.

Author contributions

MM and OAS designed this research and conduct the experiments; CDM, AL, RS, EdSR, CVcDS, RDS, DA, ASM and GG performed the experiments; TLH analyzed the data; LdRB and BB critically revised the manuscript which was reviewed by LF, AD, FS, JJVE and GN.

Funding

This project was funded by the ERC through HORIZON-HLTL-2021 project "UNDINE" (101057100); by the Italian Ministry of Research MUR program PNRR; M4-C2-I1.1 PRIN2022 "HECORES" (2022ZSLRPT) and by a contract from Nutrintech Med Italia (Rome, I), Prot. n°2885/2022) to G.N. EdSR thanks the PhD scholarship by Coordenação de Aperfeiçoamento de Pessoal de Nível Superior – Brasil (CAPES), grant number 001.

Data availability

No datasets were generated or analysed during the current study.

Declarations

Ethical approval

not applicable.

Consent for publication

Written informed consent for publication was obtained from all participants.

Competing interests

The authors declare no competing interests.

Ethical committee

not applicable.

Clinical trial number

not applicable.

Received: 14 August 2024 / Accepted: 28 August 2024

Published online: 16 October 2024

References

1. Fernandes Q, Inchakalody VP, Merhi M, Mestiri S, Taib N, Moustafa A, El-Ella D, et al. Emerging COVID-19 variants and their impact on SARS-CoV-2 diagnosis, therapeutics and vaccines. *Ann Med*. 2022;54:524–40. <https://doi.org/10.1080/07853890.2022.2031274>.
2. Cohen J. COVID-19 is surging again-with far fewer serious cases. *Science*. 2024;385:814–5. <https://doi.org/10.1126/science.ads6028>.
3. Chen X, Liu B, Li C, Wang Y, Geng S, Du X, et al. Stem cell-based therapy for COVID-19. *Int Immunopharmacol*. 2023;124:110890. <https://doi.org/10.1016/j.intimp.2023.110890>.

4. Mongin D, Bürgisser N, Laurie G, Schimmel G, Vu DL, Cullati S, et al. Effect of SARS-CoV-2 prior infection and mRNA vaccination on contagiousness and susceptibility to infection. *Nat Commun.* 2023;14:1–13. <https://doi.org/10.1038/s41467-023-41109-9>.
5. Martín Sánchez FJ, Martínez-Sellés M, Molero García JM, Moreno Guillén S, Rodríguez-Artalejo FJ, Ruiz-Galiana J, et al. Insights for COVID-19 in 2023. *Rev Esp Quimioter.* 2023;36:114–24. <https://doi.org/10.37201/req/122.2022>.
6. Mykityn AZ, Fouchier RA, Haagmans BL. Antigenic evolution of SARS Coronavirus 2. *Curr Opin Virol.* 2023;62:101349. <https://doi.org/10.1016/j.coviro.2023.101349>.
7. Peleman C, Van Coillie S, Ligthart S, Men Choi S, De Waele J, Depuydt P. Ferroptosis and pyroptosis signatures in critical COVID-19 patients cell death. *Differ.* 2023; 9, 2066–77. <https://doi.org/10.1038/s41418-023-01204-2>
8. Sun X, Liu Y, Huang Z, Xu W, Hu W, Yi L, et al. SARS-CoV-2 non-structural protein 6 triggers NLRP3-dependent pyroptosis by targeting ATP6AP1. *Cell Death Differ.* 2022;29:1240–54. <https://doi.org/10.1038/s41418-021-00916-7>.
9. Mantovani A, Morrone MC, Patrono C, Santoro MG, Schiaffino S, Remuzzi G, Bussolati G. Covid-19 Commission of the Accademia Nazionale dei Lincei. Long covid: where we stand and challenges ahead. *Cell Death Differ.* 2022;29:1891–900. <https://doi.org/10.1038/s41418-022-01052-6>.
10. Arman BY, Brun J, Hill ML, Zitzmann N, von Delft A. An update on SARS-CoV-2 clinical trial results—what we can learn for the next pandemic. *Int J Mol Sci.* 2023;25:354. <https://doi.org/10.3390/ijms25010354>.
11. Li Q, Wang Y, Sun Q, Knopf J, Herrmann M, Lin L, et al. Immune response in COVID-19: what is next? *Cell Death Differ.* 2022;6:1107–22. <https://doi.org/10.1038/s41418-022-01015-x>.
12. André S, Picard M, Cezar R, Roux-Dalvai F, Alleaume-Butaux A, Soundararmoury C, et al. T cell apoptosis characterizes severe Covid-19 disease. *Cell Death Differ.* 2022;29:1486–99. <https://doi.org/10.1038/s41418-022-00936-x>.
13. Yang Y, Wu Y, Meng X, Wang Z, Younis M, Liu Y, et al. SARS-CoV-2 membrane protein causes the mitochondrial apoptosis and pulmonary edema via targeting BOK. *Cell Death Differ.* 2022;29:1395–408. <https://doi.org/10.1038/s41418-022-00928-x>.
14. Zhu Y, Zhou W, Niu Z, Sun J, Zhang Z, Li Q, et al. Long-range enhancement of N501Y-endowed mouse infectivity of SARS-CoV-2 by the non-RBD mutations of Ins215KLRs and H655Y. *Biol. Direct.* 2022;17:14. <https://doi.org/10.1186/s13062-022-00325-x>.
15. Carlos AJ, Ha DP, Yeh DW, Van Krieken R, Tseng CC, Zhang P. The chaperone GRP78 is a host auxiliary factor for SARS-CoV-2 and GRP78 depleting antibody blocks viral entry and infection. *J Biol Chem.* 2021;296:100759. <https://doi.org/10.1016/J.JBC.2021.100759>.
16. Wei X, Pan C, Zhang X, Zhang W. Total network controllability analysis discovers explainable drugs for Covid-19 treatment. *Biol Direct.* 2023;18(55). <https://doi.org/10.1186/s13062-023-00410-9>.
17. Zhu T, Niu G, Zhang Y, Chen M, Li CY, Hao L, et al. Host-mediated RNA editing in viruses. *Biol Direct.* 2023. <https://doi.org/10.1186/s13062-023-00366-w>,18,12.
18. Zhou P, Yang X, Lou, Wang XG, Hu B, Zhang L, et al. A Pneumonia Outbreak Associated with a New Coronavirus of probable Bat Origin. *Nature.* 2020;579:270–3. <https://doi.org/10.1038/s41586-020-2012-7>.
19. Zhang Y, Sun S, Du C, Hu K, Zhang C, Liu M, et al. Transmembrane serine protease TMPRSS2 implicated in SARS-CoV-2 infection is Autoactivated intracellularly and requires N-Glycosylation for Regulation. *J Biol Chem.* 2022;298:102643. <https://doi.org/10.1016/j.jbc.2022.102643>.
20. Yamamoto M, Kiso M, Sakai-Tagawa Y, Iwatsuki-Horimoto K, Imai M, Takeda M, et al. The Anticoagulant Nafamostat Potently Inhibits SARS-CoV-2 S protein-mediated Fusion in a cell Fusion Istem and viral infection *In Vitro* in a cell-type-dependent manner. *Viruses.* 2020;12:629. <https://doi.org/10.3390/v12060629>.
21. Ibrahim IM, Abdelmalek DH, Elshahat ME, Elfiky AA. COVID-19 spike-host cell receptor GRP78 binding site prediction. *J Infect.* 2020;80:554–62. <https://doi.org/10.1016/j.jinf.2020.02.026>.
22. Mody V, Ho J, Wills S, Mawri A, Lawson L, Ebert MCCJC, et al. Identification of 3-Chymotrypsin like protease (3CLPro) inhibitors as potential Anti-SARS-CoV-2 agents. *Commun Biol.* 2021;4:93. <https://doi.org/10.1038/s42003-020-01577-x>.
23. Quimque MTJ, Notarte KIR, Fernandez RAT, Mendoza MAO, Liman RAD, Lim JAK, et al. Virtual screening-driven Drug Discovery of SARS-CoV2 enzyme inhibitors targeting viral attachment, Replication, post-translational modification and host immunity evasion infection mechanisms. *J Biomol Struct Dyn.* 2021;39:4316–33. <https://doi.org/10.1080/07391102.2020.1776639>.
24. Ramasamy S, Subbian S. Critical Determinants of Cytokine Storm and Type I Interferon Response in COVID-19 pathogenesis. *Clin Microbiol Rev.* 2021;34:1–24. <https://doi.org/10.1128/CMR.00299-20>.
25. Tomassoli I, Gündisch D. The twin drug approach for novel nicotinic acetylcholine receptor ligands. *Bioorg Med Chem.* 2015;23:4375–89. <https://doi.org/10.1016/j.bmc.2015.06.034>.
26. Ibacache JA, Faundes J, Montoya M, Mejias S, Valderrama JA. Preparation of Novel Homodimers Derived from Cytotoxic isoquinolinequinones. *Twin Drug Approach Molecules.* 2018;23:439. <https://doi.org/10.3390/molecules23020439>.
27. Zhang B, Jin Y, Zhang L, Wang H, Wang X. Ninety years of Pentamidine: the development and applications of Pentamidine and its analogs. *Curr Med Chem.* 2022;29:4602–9. <https://doi.org/10.2174/0929867329666220314121446>.
28. Huang TL, Mayence A, Vanden Eynde JJ. Some non-conventional biomolecular targets for diamidines. A short survey. *Bioorg Med Chem.* 2014;22:1983–92. <https://doi.org/10.1016/j.bmc.2014.02.049>.
29. Mayence A, Pietka A, Collins MS, Cushion MT, Tekwani BL, Huang TL, et al. Novel bisbenzimidazoles with Antileishmanial Effectiveness. *Bioorg Med Chem Lett.* 2008;18:2658–61. <https://doi.org/10.1016/j.bmcl.2008.03.020>.
30. Rodrigues L, Cunha RB, Vassilevskaia T, Viveiros M, Cunha C. Drug Repurposing for COVID-19: a review and a Novel Strategy to identify new targets and potential drug candidates. *Molecules.* 2022;27:2723. <https://doi.org/10.3390/molecules27092723>.
31. Ulm JW, Nelson SF. COVID-19 drug Repurposing: Summary statistics on current clinical trials and promising untested candidates. *Transbound Emerg Dis.* 2021;68:313–7. <https://doi.org/10.1111/tbed.13710>.
32. Spitalieri P, Centofanti F, Murdocca M, Scioli MG, Latini A, Cesare et al. Two different therapeutic approaches for SARS-CoV-2 in hiPSCs-Derived lung organoids. 2022, 11, 1235. <https://doi.org/10.3390/cells11071235>
33. Murdocca M, Citro G, Romeo I, Lupia A, Miersch S, Amadio B, Bonomo A, et al. Peptide platform as a powerful Tool in the fight against Covid-19. *Viruses.* 2021;13:1–21. <https://doi.org/10.3390/v13081667>.
34. Bastien D, Ebert MCCJC, Forge D, Toulouse J, Kadnikova N, Perron F, et al. Fragment-based design of symmetrical bis-benzimidazoles as selective inhibitors of the Trimethoprim-Resistant, type II R67 Dihydrofolate Reductase. *J Med Chem.* 2012;55:3182–92. <https://doi.org/10.1021/jm201645r>.
35. Jin Z, Du X, Xu Y, Deng Y, Liu M, Zhao Y, et al. Structure of Mpro from SARS-CoV-2 and Discovery of its inhibitors. *Nature.* 2020;582:289–93. <https://doi.org/10.1038/s41586-020-2223-y>.
36. Yang J, Nune M, Zong Y, Zhou L, Liu Q. Close and Allosteric Opening of the Polypeptide-Binding Site in a Human Hsp70 Chaperone BiP. *Structure.* 2015, 23, 2191–2203. <https://doi.org/10.1016/j.str.2015.10.012>
37. Berman HM, Westbrook J, Feng Z, Gilliland G, Bhat TN, Weissig H, et al. The Protein Data Bank. *Nucleic Acids Res.* 2000;28:235–42. <https://doi.org/10.1093/nar/28.1.235>.
38. Bayly CI, Cieplak P, Cornell WD, Kollman PAA. Well-behaved electrostatic potential based method using charge restraints for deriving atomic charges: the RESP Model. *J Phys Chem.* 1993;97:10269–80. <https://doi.org/10.1021/j100142a004>.
39. Gasteiger J, Marsili M. Iterative Partial Equalization of Orbital Electronegativity—a Rapid Access to Atomic charges. *Tetrahedron.* 1980;36:3219–28. [https://doi.org/10.1016/0040-4020\(80\)80168-2](https://doi.org/10.1016/0040-4020(80)80168-2).
40. Trott O, Olson AJ. AutoDock Vina: improving the speed and accuracy of docking with a new scoring function, efficient optimization, and Multithreading. *J Comput Chem.* 2010;31:455–61. <https://doi.org/10.1002/jcc.21334>.
41. Huang J, Rauscher S, Nawrocki G, Ran T, Feig M, De Groot BL, et al. CHARMM36m: an Improved Force Field for folded and intrinsically disordered proteins. *Nat Methods.* 2016;14:71–3. <https://doi.org/10.1038/nmeth.4067>.
42. Abraham MJ, Murtola T, Schulz R, Páll S, Smith JC, Hess B, et al. Gromacs: high performance Molecular simulations through Multi-level parallelism from laptops to supercomputers. *SoftwareX.* 2015;1–2:19–25. <https://doi.org/10.1016/j.softx.2015.06.001>.
43. Vanommeslaeghe K, Hatcher E, Acharya C, Kundu S, Zhong S, Shim J, et al. CHARMM general force field: a force field for drug-like molecules compatible with the CHARMM all-atom additive biological force fields. *J Comput Chem.* 2010;31:671–90. <https://doi.org/10.1002/jcc.21367>.CHARMM.
44. Berendsen HJC, Postma JPM, Van Gunsteren WF, Dinola A, Haak JR. Molecular Dynamics with Coupling to an external bath. *J Chem Phys.* 1984;81:3684–90. <https://doi.org/10.1063/1.448118>.

45. Parrinello M, Rahman A. Polymorphic transitions in single crystals: a New Molecular Dynamics Method. *J Appl Phys*. 1981;52:7182–90. <https://doi.org/10.1063/1.328693>.
46. Essmann U, Perera L, Berkowitz ML, Darden T, Lee H, Pedersen LG. A smooth particle Mesh Ewald Method. *J Chem Phys*. 1995;103:8577–93. <https://doi.org/10.1063/1.470117>.
47. Valdés-Tresanco MS, Valdés-Tresanco ME, Valiente PA, Moreno E, gmx_MMPBSA: A New Tool to perform end-state Free Energy calculations with GROMACS. *J Chem Theo Comp*. 2021;17:6281–91. <https://doi.org/10.1021/acs.jctc.1c00645>.
48. Daura X, Gademann K, Jaun B, Seebach D, van Gunsteren W, Mark A. Peptide folding when simulation meets experiment. *Angew Chem*. 1999;111:245–9.
49. Sander T, Freyss J, Von Korff M, Rufener C, DataWarrior. *J Chem Inf Model*. 2015;55:460–73. <https://doi.org/10.1021/ci500588j>; An Open-Source Program for Chemistry Aware Data Visualization and Analysis.
50. Pettersen EF, Goddard TD, Huang CC, Couch GS, Greenblatt DM, Meng EC, et al. UCSF Chimera - A Visualization System for Exploratory Research and Analysis. *J Comput Chem*. 2004;25:1605–12. <https://doi.org/10.1002/jcc.20084>.
51. Morris GM, Ruth H, Lindstrom W, Sanner MF, Belew RK, Goodsell DS, et al. Software News and Updates AutoDock4 and AutoDockTools4: automated docking with selective receptor flexibility. *J Comput Chem*. 2009;30:2785–91. <https://doi.org/10.1002/jcc.21256>.
52. Toulouse JL, Yachnin BJ, Ruediger EH, Deon D, Gagnon M, Saint-Jacques K, et al. Structure-based design of Dimeric Bisbenzimidazole inhibitors to an Emergent Trimethoprim-resistant type II Dihydrofolate Reductase guides the design of Monomeric Analogues. *ACS Omega*. 2019;4:10056–69. <https://doi.org/10.1021/acsomega.9b00640>.
53. Brandimarte B, Di Rienzo Businco L, Cappello F, Fiore R, Bastone G, Gualdi G, et al. Nebulization of pharmacological solutions with an innovative medical device based on microvaporization. *Heliyon*. 2023;9:e14673. <https://doi.org/10.1016/j.heliyon.2023.e14673>.
54. Li G, Hilgenfeld R, Whitley R, De Clercq E. Therapeutic strategies for COVID-19: Progress and lessons learned. *Nat Rev Drug Discov*. 2023;22:449–75. <https://doi.org/10.1038/s41573-023-00672-y>.
55. Cao B, Wang Y, Lu H, Huang C, Yang Y, Shang L. Et. Al. Oral simonotrelvir for adult patients with mild-to-moderate Covid-19. *N Engl J Med*. 2024;390:230–41. <https://doi.org/10.1056/NEJMoa2301425>.
56. Miersch S, Sharma N, Saberianfar R, Chen C, Caccuri F, Zani A. Ultrapotent and Broad neutralization of SARS-CoV-2 variants by Modular, Tetravalent, Bi-paratopic Antibodies. *Cell Rep*. 2022;39. <https://doi.org/10.1016/j.celrep.2022.110905>.
57. Labriola JM, Miersch S, Chen G, Chen C, Pavlenco A, Saberianfar R, et al. Peptide-antibody fusions Engineered by Phage Display exhibit an Ultrapotent and Broad neutralization of SARS-CoV-2 variants. *ACS Chem Biol*. 2022;17:1978–88. <https://doi.org/10.1021/acscchembio.2c00411>.
58. Pobre KFR, Poet GJ, Hendershot LM. The endoplasmic reticulum (ER) chaperone BiP is a Master Regulator of ER functions: getting by with a little help from ERdj friends. *J Biol Chem*. 2019;294:2098–108. <https://doi.org/10.1074/jbc.REV118.002804>.
59. Sabirli R, Koseler A, Goren T, Turkcuier I, Kurt O. High GRP78 levels in Covid-19 infection: a case-control study. *Life Sci*. 2021;265:118781. <https://doi.org/10.1016/j.lfs.2020.118781>.
60. Versteeg GA, van de Nes PS, Bredenbeek PJ, Spaan WJM. The Coronavirus spike protein induces endoplasmic reticulum stress and upregulation of intracellular chemokine mRNA concentrations. *J Virol*. 2007;81:10981–90. <https://doi.org/10.1128/jvi.01033-07>.
61. Glaab E, Manoharan GB, Abankwa D. A Pharmacophore Model for SARS-CoV-2 3CLpro small molecule inhibitors and in Vitro Experimental Validation of computationally screened inhibitors. *J Chem Inf Model*. 2021;61:4082–96. <https://doi.org/10.1021/acs.jcim.1c00258>.

Publisher's note

Springer Nature remains neutral with regard to jurisdictional claims in published maps and institutional affiliations.